

Quantum Analytic Descent

Bálint Koczor* and Simon C. Benjamin

Department of Materials, University of Oxford, Parks Road, Oxford OX1 3PH, United Kingdom

Quantum variational algorithms are applicable to a range of tasks and have particular relevance for near-term quantum computers. The approach involves adjusting the parameterised elements of a quantum circuit to minimise the expected energy of the output state with respect to a Hamiltonian encoding the task. Typically the parameter space is navigated by descending the steepest energy gradient at each incremental step; this can become costly as the solution is approached and all gradients vanish. Here we propose an alternative analytic descent mechanism. Given that the variational circuit can be expressed as a (universal) set of Pauli operators, we observe that the energy landscape must have a certain simple form in the local region around any reference point. By fitting an analytic function to the landscape, one can classically analyse that function in order to directly ‘jump’ to the (estimated) minimum, before fitting a more refined function if necessary. We verify this technique using numerical simulations and find that each analytic jump can be equivalent to many thousands of steps of canonical gradient descent.

An exciting era was heralded last year with the announcement of a quantum device whose behaviour cannot be simulated using classical computers with practical levels of resource [1]. In this era, quantum computers may have the potential to perform useful tasks of value to society that cannot be performed by other means. However the quantum devices are still immature by the standards of the fault-tolerant universal systems that we expect to emerge eventually. The early machines will not have a comprehensive solution to accumulating noise [2], and therefore it is a considerable and fascinating challenge to achieve a valuable function despite the imperfections. One very promising class of approaches are generically called quantum variational algorithms (QVAs). In this approach one seeks to make use of a quantum circuit of (presumably) relatively low depth [3–7], by adjusting the function it performs to tune it to the desired task.

Typically a simple-to-prepare reference state (such as all-zero) is passed into a quantum circuit, called the ansatz circuit, within which there are numerous parameterised gates. The idea exists in many variants, both theoretical and experimental [8–27]. In a typical implementation, each gate implements a unitary which is therefore also parameterised; for example

$$\exp(-i\theta\sigma_x/2) \quad (1)$$

where σ_x is the Pauli X operator acting on a given qubit, and θ is the classical parameter. For a suitably-chosen ansatz circuit and an appropriate number of independently parameterised gates, the emerging state (also called the ansatz state) may be very complex – while inevitably being restricted to a small proportion of the exponentially large Hilbert space.

A given problem, for example the challenge of finding the ground state of some molecule of interest, is encoded by deriving a Hamiltonian \mathcal{H} whose ground state represents an acceptable solution. This is of course a non-trivial challenge in itself for many systems of interest.

Importantly, this challenge is not decoupled from the task of selecting a suitable ansatz circuit, or that of choosing the initial parameters for that circuit. Assuming that all these tasks have been appropriately performed then the hope is that there exists some set of parameters, to be discovered, for which the ansatz state emerging from the circuit is indeed (acceptably close to) the desired solution state. The problem then becomes one of parameter search – there might easily be hundreds of parameters, so that techniques from classical optimisation are very relevant to the prospects of successfully finding the proper configuration.

A popular choice is gradient descent; in the basic form of this method one evaluates the gradient of energy $\langle \mathcal{H} \rangle$ with respect to each of the ansatz parameters. One then takes a ‘small step’ in the direction of steepest gradient descent, and re-evaluates the gradient. Numerous adaptations are of course possible, ranging from varying the size of the step through to more advanced protocols for obtaining a valid direction of progress [28]. A significant development has been the incorporation of the concept of natural gradient, whereby one acknowledges the distinction between the parameter space and the Hilbert space within which the ansatz state lives, and a metric is used to correct the gradient in the parameter space to the true gradient in the Hilbert space [29, 30]. This relates to the concept of imaginary time evolution as a ground state finding protocol [31].

Although much studied, gradient descent has its limitations and costs. One such difficulty relates to the fact that certain tasks, such as determining the energy of chemical systems, must be performed to a very high accuracy to be useful (e.g. chemical accuracy, equivalent to 3 or 4 decimal places [6]). This corresponds to finding the minimum of the energy landscape very perfectly, which is problematic since the gradients vanish and thus estimating them can become increasingly expensive due to shot noise [21, 28, 32].

In the present paper we study an alternative method, of particular relevance in the latter stages of a QVA when we begin to approach the minimum of the cost function.

* balint.koczor@materials.ox.ac.uk

Using an ansatz circuit within which gates correspond to Pauli strings (a universal construction), we observe that the cost function, i.e. the expected energy of the output state with respect to the problem Hamiltonian, will necessarily have certain simple properties in the local region around any reference point. Exploiting this knowledge, we sample from the ansatz circuit to fit an analytic function to the near-minimum region. Given this function, we can descend towards the minimum classically and then take a ‘large jump’ (as compared to the small incremental steps taken in generic gradient descent) direct to that point. If necessary we then repeat the procedure of refining the analytic function and jumping again, until we reach a point satisfactorily close to the true minimum. In numerical simulations of this approach, we find that a single jump can be equivalent of thousands of steps of generic gradient descent.

Results contained in this work—In this work we consider quantum gates that are generated by Pauli strings, i.e., products of local Pauli operators. This is a very common construction and allows one to form universal quantum circuits. We aim to fully determine the structure of such circuits and characterise the energy surface they span. In particular, gates generated by Pauli strings have only two distinct eigenvalues, and it is straightforward to see that as we vary the parameter θ associated with such a gate, the corresponding slice on the energy surface is simply of the form $a + b\cos\theta + c\sin\theta$. For further discussion refer to [33, 34]. It follows that the Fourier spectrum of the full energy surface is determined by 3^ν coefficients, where ν is the number of parameters. Despite the very simple structure of such functions, determining them classically is intractable. Nevertheless, we show that one could efficiently obtain – by estimating only a quadratic number of terms – a good approximation of the ansatz state that is valid in the vicinity of a reference point. The result is a finite, multivariate trigonometric series expansion, which we use to analytically approximate the energy surface and the quantum Fisher information matrix in the vicinity of our reference point.

We propose an optimisation algorithm, in which one determines a classical approximation at every iteration step by estimating only a quadratic number of coefficients using a quantum device. This energy surface is then classically optimised in an internal loop until a suitable termination criterion is met. For example, this internal loop can be terminated when the optimisation has driven the parameters too far from the reference point. Alternatively one can augment the internal loop with feedback from the quantum device, i.e., occasionally checking if the analytical approximation is still within error bounds.

We numerically simulate this approach and find that it significantly outperforms conventional natural gradient. Our contribution can be viewed as conceptually novel; we use our explicit, analytical understanding of the ansatz-state structure to significantly improve previous, gradient-based optimisation techniques. Furthermore,

such previous techniques mainly used classical computers for performing only “easy” tasks, such as determining a gradient update step. We propose to use the classical computer for more demanding tasks, i.e., iteratively finding the minimum of our classical approximation of the energy surface, while alleviating the frequent use of a quantum device. Let us now introduce the main tools used in our approach.

Expanding the ansatz circuit—We define an ansatz circuit as a CPTP mapping, and in particular, as a product of individual gate operations as

$$\Phi(\underline{\theta}) := \Phi_\nu(\theta_\nu) \dots \Phi_2(\theta_2)\Phi_1(\theta_1). \quad (2)$$

Here $\Phi_k(\theta_k)$ are parameterised quantum gates, such as in Eq. (1). We focus on quantum gates which are generated by Pauli strings as (approximately) unitary operators $\Phi_k(\theta_k)\rho \approx U\rho U^\dagger$ with $U = \exp(-i\theta_k P_k/2)$. Here P_k are products of single-qubit Pauli operators as $P_k \in \{\text{Id}, \sigma_x, \sigma_y, \sigma_z\}^{\otimes N}$. For any such ansatz circuit, we can expand every gate into the following form. First, let us fix θ_0 and express the continuous dependence of the quantum gates on the angle θ around the fixed θ_0 as

$$\Phi_k(\theta_0 + \theta) = a(\theta)\Phi_{ak} + b(\theta)\Phi_{bk} + c(\theta)\Phi_{ck}, \quad (3)$$

where $a(\theta), b(\theta) = 1 \pm \cos(\theta)$ and $c(\theta) = \sin(\theta)/2$ are simple Fourier components. The transformations can be specified via $\Phi_{ak} = \Phi_k(\theta_0)$ and via the parameter shifts $\Phi_{bk} = \Phi_k(\theta_0 + \pi/2) - \Phi_k(\theta_0 - \pi/2)$ and $\Phi_{ck} = \Phi_k(\theta_0 + \pi)$. Note that these transformations are discrete in nature, and implicitly depend on the constant θ_0 which we have fixed as a reference point. Refer to Appendix A1 for more details.

We now expand the full ansatz circuit from Eq. (2) into the above form assuming that all gates are generated by Pauli strings via Eq. (3). We again fix θ_0 and express the continuous dependence on $\underline{\theta}$ around this reference point in parameter space as

$$\Phi(\underline{\theta}_0 + \underline{\theta}) = \prod_{k=1}^{\nu} [a(\theta_k)\Phi_{ak} + b(\theta_k)\Phi_{bk} + c(\theta_k)\Phi_{ck}]. \quad (4)$$

The above product can be expanded into a sum of 3^ν terms, which is classically intractable. Nevertheless, in the following we aim to approximate this mapping via a polynomial number of *important* summands and discard the remaining, less important terms. In particular, we introduce $\delta := \|\underline{\theta}\|_\infty$, which denotes the absolute largest entry in the parameter vector. We will now expand the above quantum circuit into a quadratic number of terms in ν which introduces an error $\mathcal{O}(\sin^3 \delta)$. We stress that this is not a simple Taylor expansion of the objective function, but a truncation of a finite, multivariate trigonometric series.

We derive the explicit form of this approximate map-

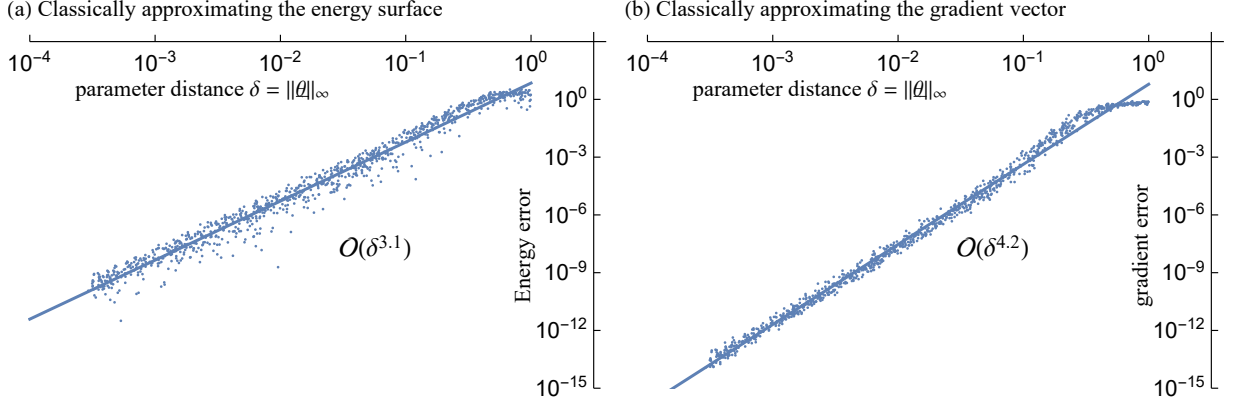


FIG. 1. Error of our trigonometric-series approximation for the energy surface (a) and gradient vector (b) as a function of the distance from the reference point $\underline{\theta}_0$ of our model. Distance $\delta = \|\underline{\theta}\|_\infty$ is given by the absolute largest entry in the parameter vector $\underline{\theta}$. As long as δ is small, we can classically approximate the gradient vector and use it in an analytic descent optimisation. The approximation error of the gradient vector is computed as the similarity measure $1 - f$, refer to text. We used the same spin-ring Hamiltonian and 84-parameter ansatz circuit as in Fig. 2, and we have included the empirical scalings of the errors as $\mathcal{O}(\delta^{3.1})$ and $\mathcal{O}(\delta^{4.2})$.

ping in Appendix A 2 as

$$\Phi(\underline{\theta}) = A(\underline{\theta})\Phi^{(A)} + \sum_{k=1}^{\nu} [B_k(\underline{\theta})\Phi_k^{(B)} + C_k(\underline{\theta})\Phi_k^{(C)}] + \sum_{l>k}^{\nu} [D_{kl}(\underline{\theta})\Phi_{kl}^{(D)}] + \mathcal{O}(\sin^3 \delta). \quad (5)$$

Here $A, B_k, C_k, D_{kl} : \mathbb{R}^\nu \mapsto \mathbb{R}$ are multivariate functions – in fact, monomials in $a(\theta), b(\theta)$ and $c(\theta)$ – and they multiply the discrete mappings as, e.g., $A(\underline{\theta})\Phi^{(A)}$. In conclusion, these monomials are products of simple univariate trigonometric functions and they completely absorb the continuous dependence on the parameters $\underline{\theta}$.

Classically computing the energy surface—A large class of potential applications of variational quantum circuits assume a target function that corresponds to *linear* mappings $E(\underline{\theta}) := \text{Tr}[\mathcal{H}\Phi(\underline{\theta})\rho_0]$, that can be used to model, e.g., the expected energy of a physical system when \mathcal{H} is a Hamiltonian. Although quantum natural gradient [28, 30, 35] allows for more general objective functions, here we only consider such linear mappings. This, nevertheless, still contains a large class of important applications, such as the variational quantum eigensolver.

Using our expansion in Eq. (5), we can express the energy surface explicitly as

$$E(\underline{\theta}) = A(\underline{\theta})E^{(A)} + \sum_{k=1}^{\nu} [B_k(\underline{\theta})E_k^{(B)} + C_k(\underline{\theta})E_k^{(C)}] + \sum_{l>k}^{\nu} [D_{kl}(\underline{\theta})E_{kl}^{(D)}] + \mathcal{O}(\sin^3 \delta). \quad (6)$$

Here $E^{(A)}, E_k^{(B)}, E_k^{(C)}, E_{kl}^{(D)} \in \mathbb{R}$ can be reconstructed by estimating the energy expectation value at discrete points in parameter space using a quantum device. For

example, $E^{(A)} = \text{Tr}[\mathcal{H}\Phi^{(A)}\rho_0] = E(\underline{\theta}_0)$ is just the energy at the fixed point $\underline{\theta}_0$ and $E_k^{(C)}$ is obtained similarly by shifting the k^{th} parameter by π , refer to Appendix B. We now only state the explicit forms of these coefficients as

$$E^{(A)} = E(\underline{\theta}_0), \quad (7)$$

$$E_k^{(B)} = E(\underline{\theta}_0 + \tfrac{1}{2}\pi \underline{v}_k) - E(\underline{\theta}_0 - \tfrac{1}{2}\pi \underline{v}_k),$$

$$E_k^{(C)} = E(\underline{\theta}_0 + \pi \underline{v}_k),$$

$$E_{kl}^{(D)} = E(\underline{\theta}_0 + \tfrac{1}{2}\pi [\underline{v}_k + \underline{v}_l]) + E(\underline{\theta}_0 - \tfrac{1}{2}\pi [\underline{v}_k + \underline{v}_l]) - E(\underline{\theta}_0 + \tfrac{1}{2}\pi [-\underline{v}_k + \underline{v}_l]) - E(\underline{\theta}_0 + \tfrac{1}{2}\pi [\underline{v}_k - \underline{v}_l]).$$

Here $\underline{v}_k \in \mathbb{R}^\nu$ denotes a standard basis vector in parameter space, e.g., $(0, 0, \dots, 0, 1, 0, \dots, 0)$. We show in Appendix B 3 that these coefficients are proportional to entries of the gradient vector and the Hessian matrix of the objective function at the point $\underline{\theta} = 0$. However, We again stress that Eq. (6) is not a simple Taylor expansion of the objective function, and hence our analytic descent approach goes beyond a Newton optimisation. In conclusion, fully determining the expansion in Eq. (6) requires one to estimate all these coefficients using a quantum device, i.e., by querying the energy expectation value at $Q = 1 + 2\nu^2 - 2\nu$ points.

Fig. 1(a) shows approximation errors obtained from a simulated ansatz circuit of 12 qubits. In our simulations we determined all the $Q = \mathcal{O}(\nu^2)$ coefficients and used them to compute the approximate energy via Eq. (6) at 1000 randomly generated points in parameter space. These randomly generated points are in the vicinity of our reference $\underline{\theta}_0$, which we choose to be close to the global optimum. We plot the approximation error as a function of the absolute largest entry in the parameter vector given by the norm $\|\underline{\theta}\|_\infty$. Fig. 1(a) confirms the error scaling $\mathcal{O}(\delta^3)$ and shows that our approximation is

very good in practice, i.e., the error is smaller than 10^{-3} as long as the parameter vector norm $\|\underline{\theta}\|_\infty$ is smaller than 0.1. We further remark that in Appendix B4 we derive exact and approximate symmetries of the energy function around local minima; the objective function is approximately reflection symmetric via $E(\underline{\theta}) \approx E(-\underline{\theta})$ and exactly reflection symmetric along slices θ_k .

Classically computing the gradient—We derive the analytic gradient of the approximate energy surface from Eq. (6) in Appendix B1 and propose an efficient classical algorithm for computing it for a given input $\underline{\theta}$ in Appendix D1. This has a classical computational complexity of $\mathcal{O}(\nu^3)$. We simulate an ansatz circuit of 12 qubits in Fig. 1(b) and compute the approximation error of the analytically calculated gradient vector. We quantify this error using the similarity measure as the normalised scalar product $f = \langle \tilde{g} | \underline{g} \rangle / (\|\tilde{g}\| \|\underline{g}\|)$, between the exact \underline{g} and the approximate \tilde{g} gradient vectors. We plot $1 - f$ in Fig. 1(b), and conclude that our approximation is very good and that our error measure scales with the parameter vector norm in fourth order as $1 - f = \mathcal{O}(\delta^4)$.

We aim to use this gradient in a classical optimisation routine (please refer to later text), but we first show that this approximation is very robust to shot noise. In particular, when using a quantum device to estimate the coefficients in Eq. (6), one needs to collect a large number of shots in order to sufficiently reduce the statistical uncertainty in those estimates. This uncertainty is quantified by the variance of the estimator, e.g., $\text{Var}[E_k^{(B)}]$ when reconstructing the coefficient $E_k^{(B)}$.

We derive the variance of the gradient estimator in Appendix B2 as

$$\text{Var}[\partial_m E(\underline{\theta})] = \left[\frac{\partial B_m(\underline{\theta})}{\partial \theta_m} \right]^2 \text{Var}[E_k^{(B)}] + \mathcal{O}(\sin^2 \delta). \quad (8)$$

This informs us that the variance of the classically computed gradient only depends on the variance of the coefficients $E_k^{(B)}$ in zeroth order – and the variance of all other estimated coefficients is scaled down quadratically by the possibly small $\delta \ll 1$. Note that the variance of our coefficients are directly proportional to the variance of estimating the energy expectation value. Advanced techniques on reducing this variance can straightforwardly be applied [36].

Metric tensor—We now show that our approximation of ansatz circuits in Eq. (4) can be used to obtain a classical model for computing how the quantum Fisher information matrix of the variational states $\rho(\underline{\theta}) := \Phi(\underline{\theta})\rho_0$ depends on the continuous parameters $\underline{\theta}$.

This metric tensor was first proposed in the context of variational quantum algorithms in [15] and has been used to improve convergence speed and accuracy of optimisations as well as to avoid local minima [29–31, 37, 38]. A general approach for optimising arbitrary quantum states was proposed in [30] via the quantum Fisher information matrix; a general approximation for noisy quantum states can be estimated via SWAP tests

as $[\mathbf{F}_Q]_{mn} = 2\text{Tr}[(\partial_m \rho(\underline{\theta}))(\partial_n \rho(\underline{\theta}))]$. Indeed, in the limit of pure states entries of this metric tensor can be estimated using Hadamard-tests [15, 29, 37]. We derive the approximation of the general matrix elements $[\mathbf{F}_Q]_{mn}$ in Appendix C; for present purposes we need only state the leading terms explicitly as, e.g.,

$$[\mathbf{F}_Q]_{mn} = \mathcal{F}_{BB} F_{BB}(\underline{\theta}) + \mathcal{F}_{AB} F_{AB}(\underline{\theta}) + \dots \mathcal{O}(\sin^2 \delta). \quad (9)$$

Here the multi-variate trigonometric functions, e.g., $F_{BB}(\underline{\theta})$, can be straightforwardly computed using the previously outlined techniques. These functions multiply the real coefficients, such as \mathcal{F}_{BB} , which can be computed from quantum-state overlaps as

$$\begin{aligned} \mathcal{F}_{BB} = & \text{Tr}[\rho(\tfrac{1}{2}\pi \underline{v}_k) \rho(\tfrac{1}{2}\pi \underline{v}_k)] + \text{Tr}[\rho(-\tfrac{1}{2}\pi \underline{v}_k) \rho(-\tfrac{1}{2}\pi \underline{v}_k)] \\ & - \text{Tr}[\rho(-\tfrac{1}{2}\pi \underline{v}_k) \rho(\tfrac{1}{2}\pi \underline{v}_k)] - \text{Tr}[\rho(\tfrac{1}{2}\pi \underline{v}_k) \rho(-\tfrac{1}{2}\pi \underline{v}_k)]. \end{aligned}$$

These overlaps $\text{Tr}[\rho(\underline{\theta}') \rho(\underline{\theta}'')]$ correspond to variational states of shifted parameters $\underline{\theta}'$ and $\underline{\theta}''$, can be estimated using SWAP tests. However, this requires the preparation of two copies of the quantum state in two separate quantum registers. Nevertheless, when the states are approximately pure as $\rho(\underline{\theta}) \approx |\psi(\underline{\theta})\rangle\langle\psi(\underline{\theta})|$, then the overlaps $|\langle\psi(\underline{\theta}')|\psi(\underline{\theta}'')\rangle|^2$, could be estimated via Hadamard tests. The latter would only require a single copy of the state.

Quantum Analytic Descent—We now use the previously outlined techniques to propose an optimisation approach for variational quantum algorithms. In particular, we assume the aim is to optimise the objective function $E(\underline{\theta}) = \text{Tr}[\mathcal{H} \rho(\underline{\theta})]$, where we have again used the notation $\rho(\underline{\theta}) = \Phi(\underline{\theta})\rho_0$. Previous gradient-based techniques assumed that one computes the gradient vector $\underline{g}(\underline{\theta})$ at every iteration using a quantum device. This gradient vector can be estimated with either Hadamard-test techniques [15, 37] or parameter-shift rules [34].

Instead, we now aim to use the explicit knowledge about the local structure of the objective function $E(\underline{\theta})$. This results in an iterative optimisation in two nested loops. In an external loop we use the quantum device to estimate the coefficients in Eq. (7). This allows us to build a classical model of the objective function locally via Eq. (6) and descend towards the minimum of this classical approximation in an internal loop. In the internal loop, we compute a classical approximation of the gradient vector at every iteration step and propagate our parameters according to a suitable update rule. We choose quantum natural gradient which applies the inverse of the metric tensor \mathbf{F}_Q to the gradient vector [29–31]. Although this metric tensor can similarly be approximated classically via Eq. (9), we remark that its quantum estimation cost becomes negligible in the vicinity of the optimum [28].

The internal, classical optimisation loop can be aided with feedback from the quantum device. There are various possibilities to implement this; one could estimate the energy with the quantum device occasionally, i.e., at

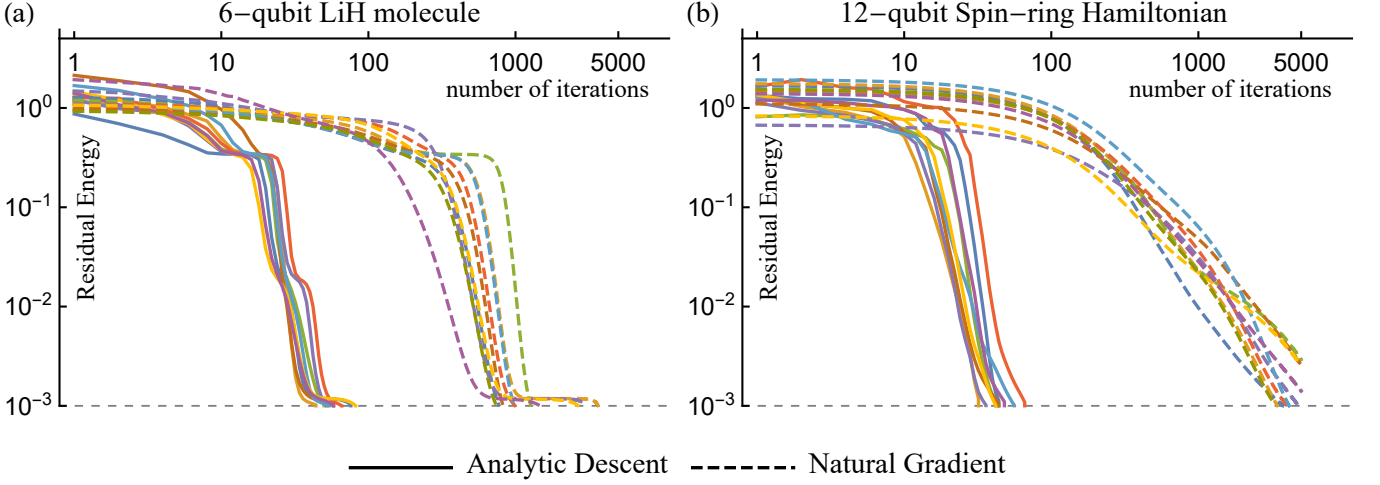


FIG. 2. Simulated analytic descent and natural gradient in the case of a molecular (a) and a spin-ring Hamiltonian (b). Plots show the distance from the exact ground-state energy as a function of the iterations. A classical approximation of the energy surface is determined at each iteration step of analytic descent (solid lines) and in an internal loop we descent towards its minimum using a classical computer (not shown here). Analytic descent (solid lines) crucially outperforms conventional natural gradient (dashed lines) and appears to increase its convergence rate (steeper slope on plots). We simulate the effect of shot noise due to finite measurements – determining one step of analytic descent requires a factor of 2 more measurements than natural gradient. Dashed grey lines show our convergence criterion 10^{-3} , which is comparable to chemical accuracy.

every t iterations, and compare the result to the classical approximation. If the deviation is too large – possibly because $\|\underline{\theta}\|_\infty$ is too large – then the internal loop should abort and the coefficients in Eq. (7) should be re-estimated using the quantum device. Another possibility for feedback would be to estimate the previously introduced similarity measure $1 - f$ between the approximate and exact gradients using the quantum device. In any case, we expect that this feedback from the quantum device only requires a negligible amount of sampling. One could of course work without feedback and abort the internal loop when $\|\underline{\theta}\|_\infty$ exceeds a certain threshold.

Numerical simulations—We numerically simulate physical Hamiltonians. We consider a hardware-efficient ansatz construction which is built of alternating layers of single-qubit X and Y rotations and two-qubit Pauli ZZ gates. We simulate the effect of shot noise in the following way. In conventional, gradient-based optimisations one would estimate entries of the gradient vector to a precision ϵ . We set this precision such that the relative uncertainty in the gradient vector is 10% as $(0.1\|\underline{g}\|)^2 = \sum_{k=1}^{\nu} \text{Var}[g_k]$, where $\text{Var}[g_k]$ is the variance of a single vector entry [28]. One could distribute measurements optimally [28], but we simply set the number of measurements such that the precision of each gradient entry is $\epsilon(g_k) = 0.1\|\underline{g}\|/\sqrt{\nu}$. In order to be able to compare this to our analytic descent technique, we determine the coefficients to the same precision $\epsilon(E_k^{(B)}) = 0.1\|\underline{g}\|/\sqrt{\nu}$ and we determine all other coefficients in Eq. (7) to a proportionally lower precision $\epsilon = 0.1\|\underline{g}\|$. Recall that we can do so because the variance

of our classical gradient estimator in Eq. (8) is dominated by the uncertainty in $E_k^{(B)}$. This way, the overall number of measurements required for analytic descent is only a factor of 2 more than determining the gradient vector.

Fig. 2(a) shows simulation results of a LiH Hamiltonian of 6 qubits. We use an ansatz circuit with 4 blocks and overall 78 parameters. We start every optimisation from a randomly selected point in parameter space that is close to the Hartree-Fock solution. In Fig. 2(solid) we only plot the external optimisation loop of analytic descent. Indeed at every step there is a classical optimisation procedure involved, for which we have used the natural gradient update rule and we aborted the internal loop when the similarity measure is low via $1 - f < 5$. We plot curves that correspond to analytic descent Fig. 2(solid) such that we propagate data points by 2 steps at every iteration – to reflect their relative measurement costs. We furthermore estimated the metric tensor and inverted it using a large regularisation parameter $\eta = 0.01$ to ensure that its measurement cost is reasonable. The step size is 0.001 (0.1) in the case of analytic descent (natural gradient).

Note that we have used a very fine step size in the case of analytical descent, which allows us to follow the natural gradient evolution of the parameters very smoothly ranging up to many thousands of conventional gradient steps per a single classical optimisation procedure (one iteration in Fig. 2). This has several advantages and keeps the evolution stable, even when the inverse of the highly singular metric tensor \mathbf{F}_Q is used.

Fig. 2(b) shows simulation results of a spin-ring Hamil-

tonian

$$\sum_{i=1}^N J[\sigma_x^{\{i\}} \sigma_x^{\{i+1\}} + \sigma_y^{\{i\}} \sigma_y^{\{i+1\}} + \sigma_z^{\{i\}} \sigma_z^{\{i+1\}}] + \sum_{i=1}^N \omega_i \sigma_z^{\{i\}},$$

and we have set $N + 1 := 1$. We randomly generate ω_i and set $J = 0.05$. We have determined the ground state of this Hamiltonian using the previously introduced ansatz circuit, which consists of 2 blocks and overall 84 parameters. Here we set the step size to 0.01 for both approaches.

Analytic descent performs better than natural gradient even when being far from the optimum point. The gradient in this case is typically large and results in large steps that quickly drive away from the reference point θ_0 . Moreover, in both Fig. 2(a) and Fig. 2(b) we observe that analytic descent crucially outperforms natural gradient. In some regions – especially when approaching the optimum – analytic descent even appears to result in an improved convergence rate (steeper slope in the figure).

Conclusion and Discussion—In this work we analytically determined how ansatz states depend on their parameters when all gates are generated by Pauli strings; although exponentially many coefficients determine a full trigonometric expansion, we propose an efficient, approximate approach for characterising the ansatz landscape in the vicinity of a reference point.

We derived explicit formulae for classically approximating the energy surface, the gradient vector and the metric tensor as a function of the ansatz parameters. This results in a novel hybrid quantum-classical optimisation scheme in which a quantum device is only occasionally used to determine a classical approximation of the energy surface. A classical optimisation routine is then used in an internal loop to descend towards the minimum of this approximate surface. As opposed to previous techniques – which relied on point-wise information – we use the explicit, analytic knowledge about the ansatz states to build a classically tractable model. We have outlined how our classical optimisation can be aided with occasional feedback from the quantum device.

We numerically simulated the ground-state search of physical Hamiltonians and observed that indeed analytical descent significantly outperforms conventional natural gradient.

There are a number of apparent, promising extensions. First, we could use the information from the previous iterations as a Bayesian prior when re-estimating our clas-

sical model in a next step. Second, we can similarly build a classical model of the metric tensor and compute it in the internal optimisation classically without using the quantum device. Third, one could sample the coefficients in Eq. (7) optimally by distributing samples according to their strengths [28]. Furthermore, during the internal optimisation loop, one could keep track of the variance of the gradient estimator, and if it becomes too sensitive to shot noise in only a few coefficients, one could collect more data with the quantum device without re-building the full model.

There are other interesting questions that we defer to future work. This includes a more detailed analysis of the effect of shot noise and other noise sources on analytic descent. Furthermore, our approach is completely general and can be applied to any Hamiltonian \mathcal{H} . However, we expect that increasingly more complex Hamiltonians – such as in quantum chemistry – might result in more complex energy surfaces which are more difficult to approximate classically. Nevertheless, our approach guarantees that the approximation error scales cubically with the distance from the reference point.

ACKNOWLEDGMENTS

SCB acknowledges financial support from EPSRC Hub grants under the agreement numbers EP/M013243/1 and EP/T001062/1, and from the IARPA funded LogiQ project. BK and SCB acknowledge funding received from EU H2020-FETFLAG-03-2018 under the grant agreement No 820495 (AQTION). The numerical modelling involved in this study made use of the Quantum Exact Simulation Toolkit (QuEST), and the recent development QuESTlink [39] which permits the user to use Mathematica as the integrated front end. The authors are grateful to those who have contributed to both these valuable tools. The views and conclusions contained herein are those of the authors and should not be interpreted as necessarily representing the official policies or endorsements, either expressed or implied, of the ODNI, IARPA, or the U.S. Government. The U.S. Government is authorized to reproduce and distribute reprints for Governmental purposes notwithstanding any copyright annotation thereon. Any opinions, findings, and conclusions or recommendations expressed in this material are those of the author(s) and do not necessarily reflect the view of the U.S. Army Research Office.

-
- [1] F. Arute, K. Arya, R. Babbush, and et al., *Nature* **574**, 505 (2019).
 - [2] J. Preskill, arXiv preprint arXiv:1801.00862 (2018).
 - [3] I. Kassal, J. D. Whitfield, A. Perdomo-Ortiz, M.-H. Yung, and A. Aspuru-Guzik, *Annual review of physical chemistry* **62**, 185 (2011).

- [4] D. Lu, B. Xu, N. Xu, Z. Li, H. Chen, X. Peng, R. Xu, and J. Du, *Phys. Chem. Chem. Phys.* **14**, 9411 (2012).
- [5] K. B. Whaley, A. R. Dinner, and S. A. Rice, *Quantum information and computation for chemistry* (John Wiley & Sons, 2014).
- [6] S. McArdle, S. Endo, A. Aspuru-Guzik, S. Benjamin, and X. Yuan, arXiv preprint arXiv:1808.10402 (2018).

- [7] B. Koczor, S. Endo, T. Jones, Y. Matsuzaki, and S. C. Benjamin, *New J. Phys.* **22**, 083038 (2020).
- [8] E. Farhi, J. Goldstone, and S. Gutmann, arXiv preprint arXiv:1411.4028 (2014).
- [9] A. Peruzzo, J. McClean, P. Shadbolt, M.-H. Yung, Q. Zhou, P. J. Love, A. Aspuru-Guzik, and J. L. O'Brien, *Nature communications* **5** (2014).
- [10] Y. Wang, F. Dolde, J. Biamonte, R. Babbush, V. Bergholm, S. Yang, I. Jakobi, P. Neumann, A. Aspuru-Guzik, J. D. Whitfield, *et al.*, *ACS nano* **9**, 7769 (2015).
- [11] P. J. J. O'Malley, R. Babbush, I. D. Kivlichan, J. Romero, J. R. McClean, R. Barends, J. Kelly, P. Roushan, A. Tranter, N. Ding, B. Campbell, Y. Chen, Z. Chen, B. Chiaro, A. Dunsworth, A. G. Fowler, E. Jeffrey, E. Lucero, A. Megrant, J. Y. Mutus, M. Neeley, C. Neill, C. Quintana, D. Sank, A. Vainsencher, J. Wenner, T. C. White, P. V. Coveney, P. J. Love, H. Neven, A. Aspuru-Guzik, and J. M. Martinis, *Phys. Rev. X* **6**, 031007 (2016).
- [12] Y. Shen, X. Zhang, S. Zhang, J.-N. Zhang, M.-H. Yung, and K. Kim, *Phys. Rev. A* **95**, 020501 (2017).
- [13] J. R. McClean, J. Romero, R. Babbush, and A. Aspuru-Guzik, *New J. Phys.* **18**, 023023 (2016).
- [14] S. Paesani, A. A. Gentile, R. Santagati, J. Wang, N. Wiebe, D. P. Tew, J. L. O'Brien, and M. G. Thompson, *Phys. Rev. Lett.* **118**, 100503 (2017).
- [15] Y. Li and S. C. Benjamin, *Phys. Rev. X* **7**, 021050 (2017).
- [16] J. I. Colless, V. V. Ramasesh, D. Dahlen, M. S. Blok, M. E. Kimchi-Schwartz, J. R. McClean, J. Carter, W. A. de Jong, and I. Siddiqi, *Phys. Rev. X* **8**, 011021 (2018).
- [17] R. Santagati, J. Wang, A. A. Gentile, S. Paesani, N. Wiebe, J. R. McClean, S. Morley-Short, P. J. Shadbolt, D. Bonneau, J. W. Silverstone, D. P. Tew, X. Zhou, J. L. O'Brien, and M. G. Thompson, *Science Advances* **4**, 10.1126/sciadv.aap9646 (2018).
- [18] A. Kandala, A. Mezzacapo, K. Temme, M. Takita, M. Brink, J. M. Chow, and J. M. Gambetta, *Nature* **549**, 242 (2017).
- [19] A. Kandala, K. Temme, A. D. Córcoles, A. Mezzacapo, J. M. Chow, and J. M. Gambetta, *Nature* **567**, 491 (2019).
- [20] C. Hempel, C. Maier, J. Romero, J. McClean, T. Monz, H. Shen, P. Jurcevic, B. P. Lanyon, P. Love, R. Babbush, A. Aspuru-Guzik, R. Blatt, and C. F. Roos, *Phys. Rev. X* **8**, 031022 (2018).
- [21] J. Romero, R. Babbush, J. R. McClean, C. Hempel, P. J. Love, and A. Aspuru-Guzik, *Quantum Science and Technology* **4**, 014008 (2018).
- [22] O. Higgott, D. Wang, and S. Brierley, arXiv preprint arXiv:1805.08138 (2018).
- [23] J. R. McClean, M. E. Kimchi-Schwartz, J. Carter, and W. A. de Jong, *Physical Review A* **95**, 042308 (2017).
- [24] J. I. Colless, V. V. Ramasesh, D. Dahlen, M. S. Blok, J. R. McClean, J. Carter, W. A. de Jong, and I. Siddiqi, arXiv preprint arXiv:1707.06408 (2017).
- [25] C. Kokail, C. Maier, R. van Bijnen, T. Brydges, M. K. Joshi, P. Jurcevic, C. A. Muschik, P. Silvi, R. Blatt, C. F. Roos, *et al.*, arXiv preprint arXiv:1810.03421 (2018).
- [26] K. Sharma, S. Khatari, M. Cerezo, and P. J. Coles, *New Journal of Physics* **22**, 043006 (2020).
- [27] M. Cerezo, K. Sharma, A. Arrasmith, and P. J. Coles, arXiv preprint arXiv:2004.01372 (2020).
- [28] B. van Straaten and B. Koczor, arXiv preprint arXiv:2005.05172 (2020).
- [29] J. Stokes, J. Izaac, N. Killoran, and G. Carleo, arXiv preprint arXiv:1909.02108 (2019).
- [30] B. Koczor and S. C. Benjamin, arXiv preprint arXiv:1912.08660 (2019).
- [31] S. McArdle, T. Jones, S. Endo, Y. Li, S. C. Benjamin, and X. Yuan, *npj Quantum Information* **5**, 1 (2019).
- [32] A. Arrasmith, L. Cincio, R. D. Somma, and P. J. Coles, arXiv preprint arXiv:2004.06252 (2020).
- [33] M. Ostaszewski, E. Grant, and M. Benedetti, arXiv preprint arXiv:1905.09692 (2019).
- [34] M. Schuld, V. Bergholm, C. Gogolin, J. Izaac, and N. Killoran, *Phys. Rev. A* **99**, 032331 (2019).
- [35] R. Sweke, F. Wilde, J. Meyer, M. Schuld, P. K. Fährmann, B. Meynard-Piganeau, and J. Eisert, arXiv preprint arXiv:1910.01155 (2019).
- [36] O. Crawford, B. van Straaten, D. Wang, T. Parks, E. Campbell, and S. Brierley, arXiv preprint arXiv:1908.06942 (2019).
- [37] X. Yuan, S. Endo, Q. Zhao, Y. Li, and S. C. Benjamin, *Quantum* **3**, 191 (2019).
- [38] D. Wierichs, C. Gogolin, and M. Kastoryano, arXiv preprint arXiv:2004.14666 (2020).
- [39] T. Jones and S. C. Benjamin, *Quantum Science and Technology* (2020).

Appendix A: Quantum gates generated by Pauli strings

1. Expressing a single gate

Let us consider a single gate in the ansatz circuit $U_k(\theta_k)$, where k indexes its position and $k \in \{1, 2, \dots, \nu\}$ with ν denoting the number of parameters. We assume that this gate is generated by a Pauli string P_k and ideally (when the gate is not noisy), it corresponds to the following unitary operator

$$U_k(\theta_k) := \exp(-i\theta_k P_k/2) = \cos[\theta_k/2]\text{Id} - i\sin[\theta_k/2]P_k, \quad (\text{A1})$$

where the second equality straightforwardly follows from the algebra $P_k^{2n} = \text{Id}$ and $P_k^{2n+1} = P_k$.

We now fix the parameter dependence of this gate at the reference point θ_0 and express the action of this gate on any quantum state using the continuous angle θ . Let us first define the quantum gate as a mapping $\Phi_k(\theta) : \mathcal{D} \mapsto \mathcal{D}$ over density operators, where \mathcal{D} denotes the set of density operators, i.e., positive, unit trace operators over the Hilbert space \mathbb{C}^{2^N} . The gate can then be expressed as a general mapping over arbitrary density matrices ρ as the

unitary conjugation $U_k(\theta_0 + \theta)\rho U_k^\dagger(\theta_0 + \theta)$, and this can be expanded into the following transformations

$$\Phi_k(\theta)\rho := U_k(\theta)U_k(\theta_0)\rho U_k^\dagger(\theta_0)U_k^\dagger(\theta) = \cos^2[\theta_k/2]\rho_{ref} + \sin^2[\theta_k/2]P_k\rho_{ref}P_k - i\cos[\theta/2]\sin[\theta/2](P_k\rho_{ref} - \rho_{ref}P_k). \quad (\text{A2})$$

Here we have used the notation $\rho_{ref} := U_k(\theta_0)\rho U_k^\dagger(\theta_0)$. The dependency on the continuous angle θ is absorbed into the following functions

$$\begin{aligned} \cos[\theta/2]^2 &= (1 + \cos[\theta])/2, \\ \cos[\theta/2]\sin[\theta/2] &= \sin[\theta]/2, \\ \sin[\theta/2]^2 &= (1 - \cos[\theta])/2. \end{aligned}$$

We can now formalise Eq. (A2) by separating it into *discrete* mappings over density matrices which are multiplied by continuous functions that depend on the parameter θ as

$$\Phi_k(\theta) = a(\theta)\Phi_{ak} + b(\theta)\Phi_{bk} + c(\theta)\Phi_{ck}. \quad (\text{A3})$$

Here the mapping depends on the parameter θ via the Fourier components $a(\theta), b(\theta), c(\theta) : \mathbb{R} \mapsto \mathbb{R}$ and we define their explicit forms as

$$a(\theta) := (1 + \cos[\theta])/2 = \mathcal{O}(1 + \theta^2), \quad (\text{A4})$$

$$b(\theta) := \sin[\theta]/2 = \mathcal{O}(\theta), \quad (\text{A5})$$

$$c(\theta) := (1 - \cos[\theta])/2 = \mathcal{O}(\theta^2), \quad (\text{A6})$$

and we have also included their scaling when approaching $\theta \rightarrow 0$. Note that we have intentionally introduced the constant shift θ_0 and, of course, our definition corresponds to the action $\Phi_k(0)[\rho] = U_k(\theta_0)\rho U_k^\dagger(\theta_0)$ for the case $\theta \rightarrow 0$. The discrete mappings Φ_{ak}, Φ_{bk} and Φ_{ck} in Eq. (A3) can be specified via their action on arbitrary density matrices as

$$\begin{aligned} \Phi_{ak}\rho &= U_k(\theta_0)\rho U_k^\dagger(\theta_0) \equiv \Phi_k(0)\rho, \\ \Phi_{bk}\rho &= -i[P_k, U_k(\theta_0)\rho U_k^\dagger(\theta_0)] = -\frac{\partial \left(U_k(\theta)U_k(\theta_0)\rho U_k^\dagger(\theta_0)U_k^\dagger(\theta) \right)}{\partial \theta} \Big|_{\theta=0} \\ &= U_k(\theta_0 + \pi/2)\rho U_k^\dagger(\theta_0 + \pi/2) - U_k(\theta_0 - \pi/2)\rho U_k^\dagger(\theta_0 - \pi/2) \equiv [\Phi_k(\pi/2) - \Phi_k(-\pi/2)]\rho, \\ \Phi_{ck}\rho &= P_k U_k(\theta_0)\rho U_k^\dagger(\theta_0) P_k^\dagger = U_k(\theta_0 + \pi)\rho U_k^\dagger(\theta_0 + \pi) \equiv \Phi_k(\pi)\rho. \end{aligned}$$

We finally conclude by recollecting their explicit forms as

$$\Phi_{ak} = \Phi_k(0), \quad \Phi_{bk} = \Phi_k(\pi/2) - \Phi_k(-\pi/2) \quad \Phi_{ck} = \Phi_k(\pi). \quad (\text{A7})$$

We can use the above expressions to express any linear mapping, such as the energy functional $\mathcal{E}(\rho) : \mathcal{D} \mapsto \mathbb{R}$, via the trace relation $\mathcal{E}(\rho) = \text{Tr}[\mathcal{H}\rho]$, which is often referred to as an expectation value, and \mathcal{H} is any Hermitian operator in the Hilbert space \mathbb{C}^{2^N} . We now consider the parametric mapping $E(\theta) : \mathbb{R} \mapsto \mathbb{R}$, which we define as $E(\theta) := [\mathcal{E} \circ \Phi_k(\theta)]\rho_0 = \mathcal{E}(\Phi_k(\theta)\rho_0)$ and we refer to it as the energy function, or energy landscape. The reference state can be, e.g., the computational zero state $\rho_0 := |\underline{0}\rangle\langle\underline{0}|$. We can express the energy function explicitly via the following Fourier series

$$E(\rho) = \text{Tr}[\mathcal{H}\Phi_k(\theta)\rho_0] = \alpha_k a(\theta) + \beta_k b(\theta) + \gamma_k c(\theta). \quad (\text{A8})$$

The Fourier coefficients $\alpha_k, \beta_k, \gamma_k \in \mathbb{R}$ can be completely determined by discrete samples of the energy function via the discrete mappings of the density matrix as

$$\alpha_k := \text{Tr}[\mathcal{H}\Phi_{ak}\rho_0] = E(0) + E(\pi) \quad (\text{A9})$$

$$\beta_k := \text{Tr}[\mathcal{H}\Phi_{bk}\rho_0] = E(\pi) \quad (\text{A10})$$

$$\gamma_k := \text{Tr}[\mathcal{H}\Phi_{ck}\rho_0] = E(\pi/2) - E(-\pi/2). \quad (\text{A11})$$

The above formula informs us that we can completely and analytically determine the full energy function $E(\theta)$, just by querying the function $E(\theta)$ at four different points as $(-\pi/2, 0, \pi/2, \pi)$. Of course Nyquist's theorem also informs us that this is suboptimal, since the Fourier spectrum of $E(\theta)$ is bounded with only 3 frequency terms present $(-1, 0, 1)$. This guarantees that querying the function $E(\theta)$ at only 3 points would be sufficient for completely reconstructing it. Note that due to our definitions, the parameter θ is shifted by the constant θ_0 and, for example, $E(0) = \text{Tr}[\mathcal{H}U_k(\theta_0)\rho_0 U_k^\dagger(\theta_0)]$.

2. Expanding the full ansatz circuit

Let us now consider the effect of the full ansatz circuit on the reference state $\rho_0 := |\underline{0}\rangle\langle\underline{0}|$ as

$$U(\underline{\theta}_0 + \underline{\theta})\rho_0 U^\dagger(\underline{\theta}_0 + \underline{\theta}), \quad \text{with} \quad U(\underline{\theta}_0 + \underline{\theta}) := U_\nu(\theta_{0,\nu} + \theta_\nu) \cdots U_2(\theta_{0,2} + \theta_2) U_1(\theta_{0,1} + \theta_1).$$

Here $\underline{\theta}_0 \in \mathbb{R}^\nu$ is a vector that represents a fixed, constant shift of the parameters, while the circuit depends continuously on the parameters $\underline{\theta} \in \mathbb{R}^\nu$.

Using results from the previous subsection, we can build an analytical model of the superoperator representation $\Phi(\underline{\theta})$ of the full ansatz circuit as the mapping

$$\Phi(\underline{\theta}) := \Phi_\nu(\theta_\nu) \cdots \Phi_2(\theta_2) \Phi_1(\theta_1) = \prod_{k=1}^\nu [a(\theta_k)\Phi_{ak} + b(\theta_k)\Phi_{bk} + c(\theta_k)\Phi_{ck}]. \quad (\text{A12})$$

The above equation expresses the full ansatz circuit and its dependence on the parameters $\underline{\theta}$. Of course fully expanding the above expression would result in a sum of 3^ν different terms. Nevertheless, we expand this into a sum and truncate the expansion such that the remaining terms are correct up to an error $\mathcal{O}(\sin^3 \delta)$. For this we define $\delta := \|\underline{\theta}\|_\infty$, to denote the absolute largest entry in the vector $\underline{\theta}$. We assume that the continuous parameters are only used to explore the vicinity of the reference point $\underline{\theta}_0$ in parameter space via a sufficiently small δ . This can be, e.g., when the reference parameters $\underline{\theta}_0$ are already a good approximation of the optimal ones as $\|\underline{\theta}_0 - \underline{\theta}_{opt}\|_\infty < \delta$ with $\delta \ll 1$ and we search for the ground state energy by optimising the continuous parameters. We define the approximate mapping as

$$\tilde{\Phi}(\underline{\theta}) := A(\underline{\theta})\Phi^{(A)} + \sum_{k=1}^\nu [B_k(\underline{\theta})\Phi_k^{(B)} + C_k(\underline{\theta})\Phi_k^{(C)}] + \sum_k \sum_{l=k+1}^\nu [D_{kl}(\underline{\theta})\Phi_{kl}^{(D)}]. \quad (\text{A13})$$

Here the functions $A(\underline{\theta})$, $B_k(\underline{\theta})$, $C_k(\underline{\theta})$ and $D_{kl}(\underline{\theta})$ absorb the dependence on the parameters $\underline{\theta}$ and $\Phi_k^{(A)}$, $\Phi_k^{(B)}$, $\Phi_k^{(C)}$ and $\Phi_{kl}^{(D)}$ are superoperators of discrete mappings. We compute the explicit form of the terms appearing in the summation in Eq. (A13) as

$$\begin{aligned} A(\underline{\theta}) \times \Phi^{(A)} &= \prod_{k=1}^\nu [a(\theta_k)\Phi_{ak}] = \mathcal{O}(1), \\ B_k(\underline{\theta}) \times \Phi_k^{(B)} &= [a(\theta_\nu)a(\theta_{\nu-1}) \cdots b(\theta_k) \cdots a(\theta_2)a(\theta_1)] \times [\Phi_{a\nu}\Phi_{a(\nu-1)} \cdots \Phi_{bk} \cdots \Phi_{a2}\Phi_{a1}] = \mathcal{O}(\theta_k), \\ C_k(\underline{\theta}) \times \Phi_k^{(C)} &= [a(\theta_\nu)a(\theta_{\nu-1}) \cdots c(\theta_k) \cdots a(\theta_2)a(\theta_1)] \times [\Phi_{a\nu}\Phi_{a(\nu-1)} \cdots \Phi_{ck} \cdots \Phi_{a2}\Phi_{a1}] = \mathcal{O}(\theta_k^2), \\ D_{kl}(\underline{\theta}) \times \Phi_{kl}^{(D)} &= \left([a(\theta_\nu)\Phi_{a\nu}] \cdots [b(\theta_k)\Phi_{bk}] \cdots [b(\theta_l)\Phi_{cl}] \cdots [a(\theta_1)\Phi_{a1}] \right) = \mathcal{O}(\theta_k \theta_l). \end{aligned}$$

The discrete mappings can be further simplified by using Eq. (A7) as

$$\Phi^{(A)} = \Phi(\underline{0}), \quad \Phi_k^{(B)} = \Phi(\tfrac{1}{2}\pi \underline{v}_k) - \Phi(-\tfrac{1}{2}\pi \underline{v}_k), \quad \Phi_k^{(C)} = \Phi(\pi \underline{v}_k) \quad (\text{A14})$$

$$\Phi_{kl}^{(D)} = \Phi(\tfrac{1}{2}\pi \underline{v}_k + \tfrac{1}{2}\pi \underline{v}_l) + \Phi(-\tfrac{1}{2}\pi \underline{v}_k - \tfrac{1}{2}\pi \underline{v}_l) - \Phi(-\tfrac{1}{2}\pi \underline{v}_k + \tfrac{1}{2}\pi \underline{v}_l) - \Phi(\tfrac{1}{2}\pi \underline{v}_k - \tfrac{1}{2}\pi \underline{v}_l), \quad (\text{A15})$$

where $\underline{v}_k \in \mathbb{R}^\nu$ denotes the standard basis vector, e.g., $(0, 0, \dots, 0, 1, 0, \dots, 0)$. We further remark that due to our definitions, the parameters $\underline{\theta}$ are shifted by the constant vector $\underline{\theta}_0$ and, for example, $\Phi(\underline{0})\rho_0 = U(\underline{\theta}_0)\rho_0 U^\dagger(\underline{\theta}_0)$.

We can quantify the error of the approximate mapping in Eq. (A13) via the trace distance of the resulting density operators and we express this as $\|\Phi(\underline{\theta})\rho - \tilde{\Phi}(\underline{\theta})\rho\|_{tr} = \mathcal{O}(\sin^3 \delta)$. We remark that our expansion in Eq. (A13) consist of a sum of $1 + \nu + \nu^2/2$ different terms and describes the variational mapping up to an error $\mathcal{O}(\sin^3 \delta)$. We could similarly expand the mapping into a sum of $\mathcal{O}(\nu^3)$ terms and have an error $\mathcal{O}(\sin^4 \delta)$ or beyond.

Appendix B: Approximating the full energy surface locally

We can express the full energy surface following our definition in the previous section and evaluating the discrete mappings

$$E(\underline{\theta}) := \text{Tr}[\mathcal{H} \Phi(\underline{\theta})\rho_0] = A(\underline{\theta})E^{(A)} + \sum_{k=1}^\nu [B_k(\underline{\theta})E_k^{(B)} + C_k(\underline{\theta})E_k^{(C)}] + \sum_k \sum_{l=k+1}^\nu [D_{kl}(\underline{\theta})E_{kl}^{(D)}] + \mathcal{O}(\sin^3 \delta). \quad (\text{B1})$$

We can express the discrete mappings as queries of the energy function at discrete points in parameter space as

$$\begin{aligned}
E^{(A)} &= \text{Tr}[\mathcal{H} \Phi^{(A)} \rho_0] = E(\underline{0}) \\
E_k^{(B)} &= \text{Tr}[\mathcal{H} \Phi_k^{(B)} \rho_0] = E(\tfrac{1}{2}\pi \underline{v}_k) - E(-\tfrac{1}{2}\pi \underline{v}_k) \\
E_k^{(C)} &= \text{Tr}[\mathcal{H} \Phi_k^{(C)} \rho_0] = E(\pi \underline{v}_k) \\
E_{kl}^{(D)} &= \text{Tr}[\mathcal{H} \Phi_{kl}^{(D)} \rho_0] = E(\tfrac{1}{2}\pi \underline{v}_k + \tfrac{1}{2}\pi \underline{v}_l) + E(-\tfrac{1}{2}\pi \underline{v}_k - \tfrac{1}{2}\pi \underline{v}_l) - E(-\tfrac{1}{2}\pi \underline{v}_k + \tfrac{1}{2}\pi \underline{v}_l) - E(\tfrac{1}{2}\pi \underline{v}_k - \tfrac{1}{2}\pi \underline{v}_l).
\end{aligned}$$

Here $\underline{v}_k \in \mathbb{R}^\nu$ denotes a standard basis vector, e.g., $(0, 0, \dots, 0, 1, 0, \dots, 0)$. Note that due to our definitions, the parameters $\underline{\theta}$ are shifted by the constant vector $\underline{\theta}_0$ and, for example, $E(\underline{0}) = \text{Tr}[\mathcal{H} U(\underline{\theta}_0) \rho_0 U^\dagger(\underline{\theta}_0)]$.

Using the above expressions, one can determine an $\mathcal{O}(\sin^3 \delta)$ approximation of the full energy surface by querying the energy function $E(\underline{\theta})$ at a total number of Q points, where

$$Q = 1 + \nu + 2\nu + 4(\nu^2/2 - \nu) = 1 + 2\nu^2 - 2\nu. \quad (\text{B2})$$

1. Expressing the gradient analytically

We now derive the dependence of the gradient vector components $g_m := \partial_m E(\underline{\theta})$ on the parameters $\underline{\theta}$ using our approximation from Eq. (B1). We can explicitly write

$$\partial_m E(\underline{\theta}) = \frac{\partial A(\underline{\theta})}{\partial \theta_m} E^{(A)} + \sum_{k=1}^{\nu} \left[\frac{\partial B_k(\underline{\theta})}{\partial \theta_m} E_k^{(B)} + \frac{\partial C_k(\underline{\theta})}{\partial \theta_m} E_k^{(C)} \right] + \sum_k \sum_{l=k+1}^{\nu} \left[\frac{\partial D_{kl}(\underline{\theta})}{\partial \theta_m} E_{kl}^{(D)} \right] + \mathcal{O}(\sin^2 \delta). \quad (\text{B3})$$

Let us first compute the derivatives of the single-variate functions from Eq. (A4) as

$$\frac{\partial a(\theta_k)}{\partial \theta_k} = -\sin[\theta_k]/2, \quad \frac{\partial b(\theta_k)}{\partial \theta_k} = \cos[\theta_k]/2, \quad \frac{\partial c(\theta_k)}{\partial \theta_k} = \sin[\theta_k]/2.$$

We now express the explicit forms compute partial derivatives of the monomials in the following. The first term is

$$\frac{\partial A(\underline{\theta})}{\partial \theta_m} = a(\theta_\nu) a(\theta_{\nu-1}) \cdots \frac{\partial a(\theta_m)}{\partial \theta_m} \cdots a(\theta_2) a(\theta_1) = \mathcal{O}(\theta_m).$$

Similarly we have

$$\frac{\partial B_k(\underline{\theta})}{\partial \theta_m} = \begin{cases} a(\theta_\nu) a(\theta_{\nu-1}) \cdots \frac{\partial b(\theta_m)}{\partial \theta_m} \cdots a(\theta_2) a(\theta_1) = \mathcal{O}(1) & \text{if } k = m \\ a(\theta_\nu) a(\theta_{\nu-1}) \cdots b(\theta_k) \cdots \frac{\partial a(\theta_m)}{\partial \theta_m} \cdots a(\theta_2) a(\theta_1) = \mathcal{O}(\theta_m \theta_k) & \text{if } k \neq m, \end{cases} \quad (\text{B4})$$

but note that here we do not assume that $k > l$. Very similarly we have

$$\frac{\partial C_k(\underline{\theta})}{\partial \theta_m} = \begin{cases} a(\theta_\nu) a(\theta_{\nu-1}) \cdots \frac{\partial c(\theta_m)}{\partial \theta_m} \cdots a(\theta_2) a(\theta_1) = \mathcal{O}(\theta_m) & \text{if } k = m \\ a(\theta_\nu) a(\theta_{\nu-1}) \cdots c(\theta_k) \cdots \frac{\partial a(\theta_m)}{\partial \theta_m} \cdots a(\theta_2) a(\theta_1) = \mathcal{O}(\theta_m \theta_k^2) & \text{if } k \neq m, \end{cases} \quad (\text{B5})$$

and we again do not assume that $k > l$. Finally,

$$\frac{\partial D_{kl}(\underline{\theta})}{\partial \theta_m} = \begin{cases} a(\theta_\nu) a(\theta_{\nu-1}) \cdots \frac{\partial b(\theta_m)}{\partial \theta_m} \cdots b(\theta_l) \cdots a(\theta_2) a(\theta_1) = \mathcal{O}(\theta_m) & \text{if } k = m \\ a(\theta_\nu) a(\theta_{\nu-1}) \cdots b(\theta_k) \cdots \frac{\partial b(\theta_m)}{\partial \theta_m} \cdots a(\theta_2) a(\theta_1) = \mathcal{O}(\theta_m) & \text{if } l = m \\ a(\theta_\nu) a(\theta_{\nu-1}) \cdots b(\theta_k) \cdots b(\theta_l) \cdots \frac{\partial a(\theta_m)}{\partial \theta_m} \cdots a(\theta_2) a(\theta_1) = \mathcal{O}(\theta_k \theta_l \theta_m) & \text{if } k \neq m \neq l. \end{cases} \quad (\text{B6})$$

One can therefore compute the full gradient vector analytically, up to an error $\mathcal{O}(\sin^2 \delta)$, via the monomials $A(\underline{\theta})$, $B_k(\underline{\theta})$, $C_k(\underline{\theta})$ and $D_{kl}(\underline{\theta})$. and the corresponding energy coefficients. These coefficients can be determined by querying the energy function at $\mathcal{O}(\nu^2)$ points as discussed in Sec. B. We propose an efficient classical algorithm for computing this gradient vector, and its computational complexity is $\mathcal{O}(\nu^3)$, refer to Sec. D 1.

2. Error propagation and variances

Using a straightforward linear error propagation formula, the variance of the gradient estimator can be computed via the following terms

$$\begin{aligned} \text{Var}[\partial_m E(\underline{\theta})] &= \left[\frac{\partial A(\underline{\theta})}{\partial \theta_m}\right]^2 \text{Var}[E^{(A)}] + \sum_{k=1}^{\nu} \left(\left[\frac{\partial B_k(\underline{\theta})}{\partial \theta_m}\right]^2 \text{Var}[E_k^{(B)}] + \left[\frac{\partial C_k(\underline{\theta})}{\partial \theta_m}\right]^2 \text{Var}[E_k^{(C)}] \right) \\ &\quad + \sum_k^{\nu} \sum_{l=k+1}^{\nu} \left(\left[\frac{\partial D_{kl}(\underline{\theta})}{\partial \theta_m}\right]^2 \text{Var}[E_{kl}^{(D)}] \right) + \mathcal{O}(\sin^4 \delta). \end{aligned}$$

Here the variances, such as $\text{Var}[E^{(A)}] = \text{Var}[E(\underline{0})]$, are directly proportional to the precision of the energy estimation. This variance scales inversely with how many times the energy estimator is sampled.

Now using the scaling of the multivariate functions from B 1, we can expand the above variance into a leading term $[\frac{\partial B_m(\underline{\theta})}{\partial \theta_m}]^2 = \mathcal{O}(1)$ and into terms that scale with δ as

$$\text{Var}[\partial_m E(\underline{\theta})] = \left[\frac{\partial B_m(\underline{\theta})}{\partial \theta_m}\right]^2 \text{Var}[E_k^{(B)}] + \mathcal{O}(\sin^2 \delta).$$

As long as the norm $\|\underline{\theta}\|_{\infty} < \delta$ is sufficiently small, the variance of the gradient vector is dominated by the variances of measuring $\text{Var}[E_k^{(B)}]$. This means that, even though one has to query the energy function at $\mathcal{O}(\nu^2)$ points, most of these queries need not be very precise. In fact, the variance of the gradient component is dominated by the precision of the $\mathcal{O}(\nu)$ queries used to determine the coefficients $E_k^{(B)}$. Conversely, the measurement cost of estimating our classical model to a high precision is dominated by estimating the coefficients $E_k^{(B)}$.

3. Relation to the gradient vector and to the Hessian matrix

One can straightforwardly show that the coefficients used to determine our approximation of the energy surface are related to partial derivatives of the energy surface. In particular, the gradient vector g_m from Eq. (B3) can be expressed exactly at the point $\underline{\theta}$ as

$$g_m = [\partial_m E(\underline{\theta})]|_{\underline{\theta}=\underline{0}} = E_m^{(B)} \left[\frac{\partial B_m(\underline{\theta})}{\partial \theta_m} \right] |_{\underline{\theta}=\underline{0}} = E_m^{(B)} / 2 = [E(\frac{1}{2}\pi v_k) - E(-\frac{1}{2}\pi v_k)] / 2. \quad (\text{B7})$$

This is the well-known parameter-shift rule, which estimates the gradient via sampling the energy function at two different points [34].

The mixed second partial derivatives can similarly be expressed exactly using Eq. (B1) as

$$[\partial_m \partial_n E(\underline{\theta})]|_{\underline{\theta}=\underline{0}} = E_{kl}^{(D)} \left[\frac{\partial^2 D_{kl}(\underline{\theta})}{\partial \theta_m \partial \theta_n} \right] |_{\underline{\theta}=\underline{0}} = E_{kl}^{(D)} / 4 \quad (\text{B8})$$

$$= [E(\frac{1}{2}\pi v_k + \frac{1}{2}\pi v_l) + E(-\frac{1}{2}\pi v_k - \frac{1}{2}\pi v_l) - E(-\frac{1}{2}\pi v_k + \frac{1}{2}\pi v_l) - E(\frac{1}{2}\pi v_k - \frac{1}{2}\pi v_l)] / 4, \quad (\text{B9})$$

when $n \neq m$ and

$$[\partial_m \partial_m E(\underline{\theta})]|_{\underline{\theta}=\underline{0}} = E^{(A)} \left[\frac{\partial^2 A(\underline{\theta})}{\partial \theta_m \partial \theta_m} \right] |_{\underline{\theta}=\underline{0}} + E_m^{(C)} \left[\frac{\partial^2 C_m(\underline{\theta})}{\partial \theta_m \partial \theta_m} \right] |_{\underline{\theta}=\underline{0}} \quad (\text{B10})$$

$$= [E_m^{(C)} - E^{(A)}] / 2 = E(\pi v_k) - E(\underline{0}). \quad (\text{B11})$$

To conclude, we express explicitly elements of the gradient vector as

$$g_m = [\partial_m E(\underline{\theta})]|_{\underline{\theta}=\underline{0}} = E_m^{(B)} / 2 \quad (\text{B12})$$

and elements of the Hessian matrix as

$$H_{mn} = [\partial_m \partial_n E(\underline{\theta})]|_{\underline{\theta}=\underline{0}} = \begin{cases} [E_m^{(C)} - E^{(A)}] / 2 & \text{if } m = n \\ E_{kl}^{(D)} / 4 & \text{if } m \neq n. \end{cases} \quad (\text{B13})$$

This means that when querying the energy function in Sec. B and in Sec. B 1, the information we determine is very closely related to the Hessian and the gradient of the energy surface. However, we stress that our approximation is not a simple Taylor expansion.

4. Symmetry of the energy surface around the optimum

At a local optimum one finds that the gradient vanishes as $g_m = 0$ for $m \in \{1, \dots, \nu\}$. We set $\underline{\theta}_0 := \underline{\theta}_{opt}$ and therefore $\underline{\theta} = 0$. The explicit form of the leading terms in the energy surface can be expressed as

$$E(\underline{\theta}) := \text{Tr}[\mathcal{H} \Phi(\underline{\theta}) \rho_0] = A(\underline{\theta}) E^{(A)} + \sum_{k=1}^{\nu} [C_k(\underline{\theta}) E_k^{(C)}] + \sum_k \sum_{l=k+1}^{\nu} [D_{kl}(\underline{\theta}) E_{kl}^{(D)}] + \mathcal{O}(\sin^3 \delta). \quad (\text{B14})$$

and we have used that $E_k^{(B)} = 0$ due to $g_k = 0$. We now make two observations which pose strict constraints on the geometry of the energy surface around local optima. First, the energy function in this case is (approximately) reflection symmetric via

$$E(\underline{\theta}) = E(-\underline{\theta}) + \mathcal{O}(\sin^3 \delta), \quad (\text{B15})$$

due to the reflection symmetry of the basis functions $A(\underline{\theta})$, $C_k(\underline{\theta})$ and $D_{kl}(\underline{\theta})$. Second, any slice of the energy function is just a shifted cosine function as

$$E(\theta_k \underline{v}_k) = E^{(A)}(1 + \cos[\theta_k])/2 + E_k^{(C)}(1 - \cos[\theta_k])/2, \quad (\text{B16})$$

which can be written as $a + b \cos(\theta_k)$ and $a = E^{(A)} + E_k^{(C)}$, while $b = E^{(A)} - E_k^{(C)}$.

Appendix C: Expanding the metric tensor entries

It was shown in [30] that the quantum Fisher information matrix can be approximated by the scalar product

$$[\mathbf{F}_Q]_{mn} = 2\text{Tr}\left[\frac{\partial \rho(\underline{\theta})}{\partial \theta_m} \frac{\partial \rho(\underline{\theta})}{\partial \theta_n}\right], \quad (\text{C1})$$

which relation becomes exact in the limit of pure states. Here we have denoted $\rho(\underline{\theta}) := \Phi(\underline{\theta}) \rho_0$. We can straightforwardly express the partial derivatives via the partial derivative of the mapping

$$\frac{\partial \rho(\underline{\theta})}{\partial \theta_m} = \frac{\partial \Phi(\underline{\theta})}{\partial \theta_m} \rho_0 = \frac{\partial \tilde{\Phi}(\underline{\theta})}{\partial \theta_m} \rho_0 + \mathcal{O}(\sin^3 \delta), \quad (\text{C2})$$

which we aim to express explicitly using our approximate mapping $\tilde{\Phi}(\underline{\theta})$ from Eq. (A13). We can compute the derivative analytically as

$$\frac{\partial \tilde{\Phi}(\underline{\theta})}{\partial \theta_m} = \frac{\partial A(\underline{\theta})}{\partial \theta_m} \Phi^{(A)} + \sum_{k=1}^{\nu} \left[\frac{\partial B_k(\underline{\theta})}{\partial \theta_m} \Phi_k^{(B)} + \frac{\partial C_k(\underline{\theta})}{\partial \theta_m} \Phi_k^{(C)} \right] + \sum_k \sum_{l=k+1}^{\nu} \left[\frac{\partial D_{kl}(\underline{\theta})}{\partial \theta_m} \Phi_{kl}^{(D)} \right] + \mathcal{O}(\sin^2 \delta). \quad (\text{C3})$$

and note that this expression is directly analogous to the gradient vector from Eq. (B3), and we have defined the partial derivatives of the monomials, such as $\frac{\partial A(\underline{\theta})}{\partial \theta_m}$, in Sec. B 1. Expanding the quantum Fisher information to leading terms only results in

$$[\mathbf{F}_Q]_{mn} = \mathcal{F}_{BB} F_{BB}(\underline{\theta}) + \mathcal{F}_{AB} F_{AB}(\underline{\theta}) + \dots + \mathcal{O}(\sin^2 \delta). \quad (\text{C4})$$

We do not write out all the terms explicitly for clarity – however, note that they could be computed straightforwardly.

Similarly as before, we have monomials that completely absorb the continuous dependence on the parameters $\underline{\theta}$ and their explicit forms can be computed as

$$F_{BB}(\underline{\theta}) := 2 \frac{\partial B_m(\underline{\theta})}{\partial \theta_m} \frac{\partial B_n(\underline{\theta})}{\partial \theta_n} \quad (\text{C5})$$

$$F_{AB}(\underline{\theta}) := 2 \frac{\partial B_m(\underline{\theta})}{\partial \theta_m} \frac{\partial A(\underline{\theta})}{\partial \theta_n} + 2 \frac{\partial A(\underline{\theta})}{\partial \theta_m} \frac{\partial B_n(\underline{\theta})}{\partial \theta_n} \quad (\text{C6})$$

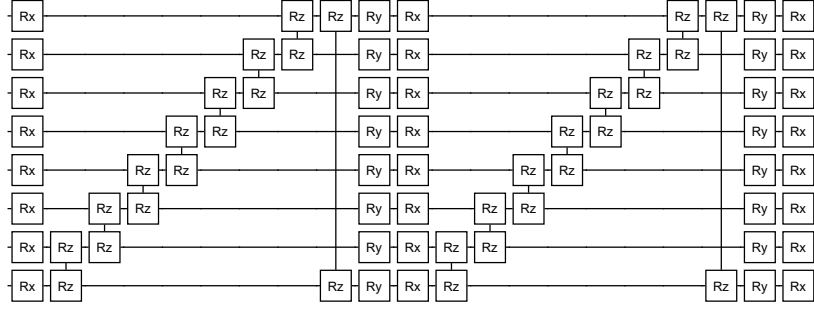


FIG. 3. Example of a 2-block ansatz circuit of 8 qubits. We used 4-block circuits in our simulations.

These functions multiply the coefficients, e.g., $\text{Tr}[(\Phi^{(B)}\rho_0)(\Phi^{(B)}\rho_0)]$, which can be computed via the discrete transformations as

$$\mathcal{F}_{BB} = \text{Tr}[(\Phi^{(B)}\rho_0)(\Phi^{(B)}\rho_0)] = \text{Tr}[\rho(\frac{1}{2}\pi v_k)\rho(\frac{1}{2}\pi v_k)] + \text{Tr}[\rho(-\frac{1}{2}\pi v_k)\rho(-\frac{1}{2}\pi v_k)] \quad (\text{C7})$$

$$- \text{Tr}[\rho(-\frac{1}{2}\pi v_k)\rho(\frac{1}{2}\pi v_k)] - \text{Tr}[\rho(\frac{1}{2}\pi v_k)\rho(-\frac{1}{2}\pi v_k)] \quad (\text{C8})$$

$$\mathcal{F}_{AB} = \text{Tr}[(\Phi^{(A)}\rho_0)(\Phi^{(B)}\rho_0)] = \text{Tr}[\rho(0)\rho(\frac{1}{2}\pi v_k)] - \text{Tr}[\rho(0)\rho(-\frac{1}{2}\pi v_k)]. \quad (\text{C9})$$

The coefficients therefore can be estimated by estimating the overlap between the states, as e.g., $\rho(0)$ and $\rho(\frac{1}{2}\pi v_k)$. These can be straightforwardly estimated using SWAP tests or, in the case of pure states, using Hadamard tests as, e.g.,

$$\text{Tr}[\rho(0)\rho(\frac{1}{2}\pi v_k)] = |\langle\psi(0)|\psi(\frac{1}{2}\pi v_k)\rangle|^2. \quad (\text{C10})$$

Appendix D: Numerical simulations

1. Classical algorithm for computing the gradient vector

We now describe how the analytical gradient from Eq. (B3) can be computed classically efficiently. We assume the the coefficients $E^{(A)}, E_k^{(B)}, E_k^{(C)}, E_{kl}^{(D)}$ are already determined and accessible in RAM. This requires $\mathcal{O}(\nu^2)$ space, which is reasonable for up to thousands of parameters.

First our classical algorithm needs to compute the monomials, e.g., $\frac{\partial A(\underline{\theta})}{\partial \theta_m}$ for a given input vector $\underline{\theta}$. We do this by precomputing and storing the basis functions $a(\theta_k), b(\theta_k) = 1 \pm \cos(\theta_k)$ and $c(\theta_k) = \sin(\theta_k)/2$ and

$$\frac{\partial a(\theta_k)}{\partial \theta_k} = -\sin[\theta_k]/2, \quad \frac{\partial b(\theta_k)}{\partial \theta_k} = \cos[\theta_k]/2, \quad \frac{\partial c(\theta_k)}{\partial \theta_k} = \sin[\theta_k]/2,$$

for all parameters $k \in \{1, \dots, \nu\}$. This is done in $\mathcal{O}(\nu)$ time and requires only $\mathcal{O}(\nu)$ storage space.

In the next step we multiply the basis functions to obtain $A(\underline{\theta})$ as

$$A(\underline{\theta}) = a(\theta_1)a(\theta_2)\cdots a(\theta_\nu),$$

and store it. All other monomials are obtained from this just by dividing it by, e.g., $a(\theta_k)$, and then multiplying it with, e.g., $\frac{\partial b(\theta_k)}{\partial \theta_k}$, which we have already precomputed. For example, the monomial $\frac{\partial B_k(\underline{\theta})}{\partial \theta_m}$ is obtained as

$$\frac{\partial B_k(\underline{\theta})}{\partial \theta_m} = \frac{A(\underline{\theta})}{a(\theta_k)a(\theta_m)} \frac{\partial b(\theta_m)}{\partial \theta_m} b(\theta_k),$$

when $k \neq m$ and note that we have already precomputed all components in the above equation. In conclusion, evaluating all $\nu Q = \mathcal{O}(\nu^3)$ basis functions in the gradient vector for a given input vector $\underline{\theta}$ can be done in $Q = \mathcal{O}(\nu^3)$ and requires $\mathcal{O}(\nu^2)$ storage.

2. Simulated optimisation

We use the ansatz circuit structure shown in Fig. 3 in our simulations. This consists of layers of single-qubit X and Y rotations as well as layers of two-qubit Pauli ZZ gates.

We consider a 6-qubit Hamiltonian of the LiH molecule. We use an ansatz circuit with 4 blocks and overall 78 parameters and start the optimisation at the vicinity of the Hartree-Fock solution. We do so by adding uniform random numbers $(-0.5, 0.5)$ to the initial parameters of the Hartree-Fock solution. The step size is 0.001 (0.1) in the case of analytic descent (natural gradient). We also determine the metric tensor at every iteration step and regularise it with a large $\eta = 0.01$.

We also consider a 12-qubit spin-ring Hamiltonian

$$\sum_{i=1}^N J[\sigma_x^{\{i\}} \sigma_x^{\{i+1\}} + \sigma_y^{\{i\}} \sigma_y^{\{i+1\}} + \sigma_z^{\{i\}} \sigma_z^{\{i+1\}}] + \sum_{i=1}^N \omega_i \sigma_z^{\{i\}},$$

in which we have set $N + 1 = 1$. We randomly generate ω_i and set $J = 0.05$. We use an ansatz circuit of 2 blocks and overall 84 parameters. We start the optimisation from the lowest energy computational basis state by adding uniform random numbers $(-0.5, 0.5)$ to its parameters. The step size is 0.01 (0.01) in the case of analytic descent (natural gradient).

We simulate shot noise when determining the gradient vector (in case of conventional natural gradient) and the coefficients in Eq. (7). We do so by adding Gaussian distributed random numbers to their exactly determined values, as discussed in the main text.